Journal of Robotics and Control (JRC)
Volume 6, Issue 4, 2025
ISSN: 2715-5072, DOI: 10.18196/jrc.v6i4.27251 2021

Lyapunov Truncation for Low-Order Modeling of Linear Time-Invariant Unmanned Rotorcraft Flight Dynamics

Ngoc-Hoi Le [1], Van-Cuong Pham [2], Dinh-Chung Dang [3], Thi-Mai-Huong Nguyen [4*]
[1] Industrial University of Ho Chi Minh City, Vietnam
[2, 3] Hanoi University of Industry, Hanoi, Vietnam
[4] Thai Nguyen University of Technology, Thai Nguyen, Vietnam
Email: [1] lengochoi@iuh.edu.vn, [2] cuongpv0610@haui.edu.vn, [3] chungdd@haui.edu.vn, [4] nguyenthimaihuong79@tnut.edu.vn
*Corresponding Author

***Abstract*—This study addresses model order reduction for unmanned rotorcraft flight dynamics, specifically focusing on the development of computationally efficient, low-order representations for fourth-order linear time-invariant (LTI) models. The research contribution is a systematic evaluation of the Lyapunov Truncation (LT) algorithm in the context of rotorcraft dynamics, where the need for reduced-order models is motivated by real-time control and simulation requirements in autonomous aerial vehicles. The LT method exploits controllability and observability Gramians to identify dominant state directions, but it inherently relies on the assumptions of linearity and time-invariance. The reduction process yields models of third, second, and first order, which are comparatively assessed using time-domain (RMSE), peak error, frequency-domain (total error), and statistical reliability metrics. Results show that the second-order reduced model achieves a 50% reduction in system complexity, with RMSE as low as 0.0537 rad/s in the lateral-to-pitch channel and relative errors consistently below 200% for all channels. Maximum deviations remain under one unit for most channels, and total frequency-domain error is minimized at this order (1519.48). In contrast, first-order models exhibit RMSEs exceeding 1000% in certain channels and peak deviations above 4 units, highlighting limitations in preserving stability margins and transient behaviors. Overall, the study demonstrates that second-order Lyapunov Truncation achieves the optimal balance between computational efficiency and dynamic fidelity, supporting its adoption for practical control-oriented reduction of LTI unmanned rotorcraft models within their valid operational envelope.**

Keywords—Model Order Reduction; Lyapunov Truncation; Flight Dynamics; Linear Time-Invariant Systems; Gramian-Based Reduction; Stability Preservation; Unmanned Rotorcraft; Lyapunov Equation.

I. INTRODUCTION

Unmanned rotorcraft systems, including quadrotors, coaxial helicopters, and tilt-rotor platforms, exemplify a class of aerial vehicles capable of vertical takeoff, hovering, and agile maneuvering, owing to their rotary-wing configurations and the absence of onboard pilots [1], [2]. These systems have been pivotal in expanding applications such as infrastructure inspection, environmental monitoring, and urban air mobility [3], [4]. The operational flexibility of rotorcraft enables rapid response in disaster management, search and rescue, and hazardous area reconnaissance [5], [6], supporting missions where adaptability and autonomy are critical [7], [8], [9]. Advances in sensor integration, multi-agent coordination, and real-time control have facilitated deployment in collaborative transport, persistent surveillance, and aerial manipulation, reinforcing the strategic role of rotorcraft in both civil and defense domains [10], [11], [12].

The development of accurate flight dynamics models is fundamental to ensuring the safety, reliability, and advanced functionality of unmanned rotorcraft [13], [14]. High-fidelity dynamic models capture complex aerodynamic, rotor, and environmental interactions [15], [16], underpinning robust control, guidance, and navigation [17], [18]. Such models are essential for simulation-based design, hardware-in-the-loop testing, and operational planning [19], [20], [21]. Additionally, dynamic modeling supports energy management, fault detection, and assessment of novel airframe or payload configurations [22], [23], [24]. The increasing demands of safety-critical and autonomous missions heighten the need for validated dynamic models integrated with adaptive and intelligent control strategies [25], [26], [27]. Techniques such as fuzzy logic, neural networks, and sliding mode control further enhance system resilience and mission success [28], [29], [30].

However, the analysis and computation of high-order flight dynamics models remain challenging due to intricate coupling among aerodynamic, multibody, and control dynamics [31], [32]. Capturing nonlinear phenomena, including rotor flapping, dynamic inflow, and fuselage-rotor interactions, often leads to high-dimensional, stiff systems with numerous state variables [33], [34]. This complexity is exacerbated by the need to model diverse operational regimes, such as transition flight, aggressive maneuvers, and disturbance rejection, each requiring accurate representation of time-varying parameters and uncertainties [35], [36], [37]. Traditional system identification and simulation approaches frequently struggle to balance model fidelity with computational efficiency, particularly for real-time analysis and certification [38], [39], [40].

In response, recent research has increasingly integrated advanced computational techniques, data-driven modeling, and robust control [41], [42]. Surrogate modeling, leveraging neural networks and reduced-order strategies, has been

successful in capturing dominant system dynamics while alleviating computational burdens [43], [44], [45]. Adaptive mesh refinement and generalized stability analysis have improved the scalability and reliability of high-order simulations [46], [47]. Control methods such as geometric trajectory planning, disturbance observers, and sliding mode control are now widely used to maintain stability and tracking under uncertainty [48], [49], [50]. Sparse identification, polytopic modeling, and nonlinear model predictive control have further supported real-time, high-performance control [51], [52]. Kinematically exact inverse-simulation algorithms and advanced actuator modeling contribute to the reliable validation of complex flight profiles [53], [54], [55]. These advances are critical in overcoming the challenges posed by high-order, high-dimensional models, promoting safer and more autonomous aerial systems [56].

Model order reduction (MOR) techniques have thus become indispensable in rotorcraft modeling, aiming to balance dynamic fidelity and computational efficiency [57], [58], [59]. Among these, the Lyapunov Truncation (LT) algorithm has been widely recognized for its theoretical foundations and practical utility in reducing the order of high-dimensional linear time-invariant (LTI) systems [60], [61]. LT utilizes controllability and observability Gramians, computed via Lyapunov equations, to eliminate state directions with minimal influence on input-output behavior [62], [63]. This reduction preserves essential dynamic characteristics and can offer error bounds under certain conditions [64], [65], [66]. LT has been effectively applied to complex models where simulation and controller synthesis are computationally demanding [67], [68]. However, the applicability of LT is inherently limited to LTI systems, typically linearized about specific operating points [69], [70]. Critical limitations, such as reduced performance in capturing rapid transients, difficulty handling time-varying or nonlinear dynamics, sensitivity to parameter variations, and numerical challenges in Gramian computation for very high-order systems, must be acknowledged [71], [72], [73]. These issues are particularly relevant for rotorcraft, where diverse and changing flight regimes and strong coupling effects are prevalent [74], [75].

Alternative MOR methods, including balanced truncation, Hankel-norm approximation, Krylov subspace approaches, and proper orthogonal decomposition, have also been explored [76], [77]. Each method presents unique strengths and drawbacks in terms of error properties, passivity preservation, and computational complexity [78], [79], [80]. Compared to these, LT offers a compelling compromise between model simplicity, stability preservation, and accuracy in moderately sized LTI systems [81]. However, previous studies have rarely examined LT's robustness to transient phenomena, error accumulation across regimes, or sensitivity in parameter-varying contexts [82], [83]. The broader literature lacks comprehensive, quantitative benchmarks of LT-reduced rotorcraft models that explicitly address these issues [84], [85].

This research thus seeks to address a critical gap in the current literature: there remains a need for systematic evaluation of the stability-preserving capabilities, accuracy, and practical limitations of LT-based model reduction for unmanned rotorcraft flight dynamics [86]. The present study rigorously applies the LT algorithm to a fourth-order LTI rotorcraft model, analyzing reduced models of various orders in both time and frequency domains. Explicit attention is given to the preservation of stability margins, error behavior across channels, and sensitivity to key parameters.

The research contribution is a comprehensive, quantitative, and qualitative assessment of Lyapunov Truncation for order reduction in LTI rotorcraft dynamics, delineating the achievable balance between computational efficiency and dynamic fidelity, and clarifying the operational boundaries and research questions, such as whether second-order LT reduction can achieve RMSE below 0.054 rad/s in lateral-to-pitch channels, maintain relative errors below 200%, and limit peak deviation within one unit while halving model complexity.

II. LYAPUNOV TRUNCATION (LT) ALGORITHM

The Lyapunov Truncation (LT) algorithm is a principled model order reduction technique for continuous-time linear time-invariant (LTI) systems. By leveraging the solutions of the system's controllability and observability Lyapunov equations, LT systematically identifies and retains the most dynamically significant state components, yielding a reduced-order model that faithfully preserves the essential input-output behavior of the original high-order system. This method is particularly valuable in contexts where preserving stability and dominant energy modes is critical, such as in robust control design and large-scale system simulation [74] – [83]. Let the original continuous-time LTI system be represented in the state-space form as follows (1):

$$\mathcal{S}_o: \begin{cases} \dot{\boldsymbol{z}}_o(t) = \boldsymbol{A}_o \boldsymbol{z}(t) + \boldsymbol{B}_o \boldsymbol{u}(t) \\ \boldsymbol{y}_o(t) = \boldsymbol{C}_o \boldsymbol{z}(t) + \boldsymbol{D}_o \boldsymbol{u}(t) \end{cases} \tag{1}$$

where $\boldsymbol{A}_o \in \mathbb{R}^{n\times n}$, $\boldsymbol{B}_o \in \mathbb{R}^{n\times m}$, $\boldsymbol{C}_o \in \mathbb{R}^{p\times n}$, and $\boldsymbol{D}_o \in \mathbb{R}^{p\times m}$. The objective of LT is to construct a reduced-order system (2):

$$\mathcal{S}_l: \begin{cases} \dot{\mathbf{z}}_l(t) = \mathbf{A}_l \mathbf{z}_l(t) + \mathbf{B}_l \mathbf{u}(t) \\ \mathbf{y}_l(t) = \mathbf{C}_l \mathbf{z}_l(t) + \mathbf{D}_l \mathbf{u}(t) \end{cases} \tag{2}$$

with $A_l \in \mathbb{R}^{l\times l}$, $B_l \in \mathbb{R}^{l\times m}$, $C_l \in \mathbb{R}^{p\times l}$, $D_l = D_o$, and $l < n$, such that the input-output behavior of $\mathcal{S}_l$ approximates that of $\mathcal{S}_o$ with high fidelity.

The LT algorithm is described as follows [74] – [83]:

Inputs: The system matrices $(\boldsymbol{A}_o, \boldsymbol{B}_o, \boldsymbol{C}_o, \boldsymbol{D}_o)$ and the desired reduced order l.

Outputs: The reduced-order system matrices $(\boldsymbol{A}_l, \boldsymbol{B}_l, \boldsymbol{C}_l, \boldsymbol{D}_l)$.

LT Algorithmic Procedure

Step 1: The algorithm commences by computing the controllability and observability Gramian matrices, denoted by $\boldsymbol{K}_c$ and $\boldsymbol{K}_o$, as the unique positive definite solutions to the following Lyapunov equations (3) and (4):

$$\boldsymbol{A}_o \boldsymbol{K}_c + \boldsymbol{K}_c \boldsymbol{A}_o^\top + \boldsymbol{B}_o \boldsymbol{B}_o^\top = \mathbf{0} \tag{3}$$

$$\boldsymbol{A}_o^{\top}\boldsymbol{K}_o + \boldsymbol{K}_o\boldsymbol{A}_o + \boldsymbol{C}_o^{\top}\boldsymbol{C}_o = \boldsymbol{0} \tag{4}$$

Step 2: To identify the most energetically significant state directions, the algorithm performs a congruence transformation based on the joint structure of $\boldsymbol{K}_c$ and $\boldsymbol{K}_o$. Specifically, the symmetric product $\boldsymbol{K}_c\boldsymbol{K}_o$ is subjected to an eigenvalue decomposition as (5):

$$\boldsymbol{K}_c\boldsymbol{K}_o = \boldsymbol{V}_{LT}\boldsymbol{\Sigma}_{LT}^2\boldsymbol{V}_{LT}^{-1} \tag{5}$$

where $\boldsymbol{V}_{LT}$ contains the generalized eigenvectors and $\boldsymbol{\Sigma}_{LT} = \mathrm{diag}(\chi_1, \dots, \chi_n)$ is the diagonal matrix of positive singular values, ordered such that $\chi_1 \geq \chi_2 \geq \cdots \geq \chi_n > 0$. The LT transformation matrix is then constructed as (6):

$$\boldsymbol{T}_{LT} = \boldsymbol{K}_c^{1/2}\boldsymbol{V}_{LT}\boldsymbol{\Sigma}_{LT}^{-1/2} \tag{6}$$

This transformation simultaneously diagonalizes both Gramians in the transformed coordinates.

Step 3: The dominant subspace is determined by selecting the first l columns of $\boldsymbol{T}_{LT}$, denoted as $\boldsymbol{T}_{LT,l}$. The original state is projected onto this subspace (7):

$$\boldsymbol{z}_l(t) = \boldsymbol{T}_{LT,l}^{\top}\boldsymbol{z}(t) \tag{7}$$

Step 4: The reduced-order system matrices are given by the following projections (8):

$$\begin{gathered}\boldsymbol{A}_l = \boldsymbol{T}_{LT,l}^{\top}\boldsymbol{A}_o\boldsymbol{T}_{LT,l};\ \boldsymbol{B}_l = \boldsymbol{T}_{LT,l}^{\top}\boldsymbol{B}_o; \\ \boldsymbol{C}_l = \boldsymbol{C}_o\boldsymbol{T}_{LT,l};\ \boldsymbol{D}_l = \boldsymbol{D}_o\end{gathered} \tag{8}$$

These matrices define the reduced-order model $\mathcal{S}_l$, which retains the most significant dynamical features of the original system.

The Lyapunov Truncation algorithm thus yields a reduced-order model by identifying and preserving the state directions associated with the largest joint controllability/observability energies, as quantified by the dominant singular values of $\boldsymbol{K}_c\boldsymbol{K}_o$. The systematic use of the LT transformation ensures that the reduced system not only approximates the original input-output map but also inherits key stability and structural properties.

While the LT algorithm offers a principled framework for model order reduction, it is crucial to recognize its intrinsic limitations and underlying assumptions to ensure scientific rigor and practical applicability. The LT algorithm is strictly limited to LTI systems. As such, its theoretical guarantees, including the preservation of stability and approximation of input-output behavior, do not generally extend to nonlinear or time-varying systems, which are common in real-world rotorcraft dynamics. Applying LT to a system outside the LTI class may result in significant modeling errors, or misrepresentation of transient and frequency-domain responses.

Another critical assumption of LT is the existence of unique, positive definite controllability and observability Gramians, $\boldsymbol{K}_c$ and $\boldsymbol{K}_o$. This presupposes that the original system is minimal, i.e., both controllable and observable. In high-order or poorly excited systems, Gramians can be ill-conditioned or nearly singular, especially when some state variables have little impact on the input-output dynamics. Such numerical difficulties can degrade the accuracy of the reduced model. Additionally, computing Gramians for very large-scale systems may pose significant computational challenges, requiring efficient numerical solvers and possibly low-rank approximations.

The selection of the truncation order l is nontrivial and can substantially affect the trade-off between model simplicity and fidelity. While the dominant singular values of $\boldsymbol{K}_c\boldsymbol{K}_o$ provide a qualitative guide, a more systematic criterion involves selecting the smallest l such that $\frac{\sum_{i=1}^{l}\chi_i}{\sum_{i=1}^{n}\chi_i} \geq \gamma$, where χ_i are the ordered singular values and $\gamma \in (0,1)$ is a chosen energy retention threshold (e.g., 0.95). However, no universal rule exists for optimal selection, and in safety-critical contexts, a posteriori validation, such as time/frequency-domain analysis or stability margin checks, remains essential.

It is important to note that LT does not guarantee the preservation of structural properties such as passivity, dissipativity, or specific frequency-domain characteristics, unless additional constraints or post-hoc verification are imposed. Therefore, verification of these properties in the reduced model is recommended, especially in aerospace or safety-critical domains.

Comparison with other model reduction techniques reveals that Modal Truncation retains eigenmodes with the slowest decay rates but may fail to capture joint input-output significance. Moment Matching methods (e.g., Krylov subspace approaches) focus on matching Markov parameters or system moments at specific frequencies, typically offering superior performance for frequency-localized approximations but less robust stability preservation. LT strikes a balance between interpretability, computational simplicity, and stability preservation in moderately sized LTI systems, but may be suboptimal in contexts requiring guaranteed passivity or extremely high-order reduction.

III. Apply Lyapunov Truncation to Reduce the Order of Unmanned Rotorcraft Systems

A precise mathematical representation of unmanned rotorcraft flight dynamics is essential for the design, analysis, and reduction of control-oriented models. In this context, the dynamics are typically expressed in a linear time-invariant (LTI) state-space framework, which is particularly well-suited for model reduction techniques such as Lyapunov Truncation (LT). Consider the linear dynamic system of the helicopter [85], [86] around the equilibrium point, which is captured by the state-space model (1), where:

$\boldsymbol{z}(t) \in \mathbb{R}^n$: State vector, $\boldsymbol{z}(t) = [\xi_1, \xi_2, \xi_3, \xi_4]^{\top}$, where ξ_1 and ξ_2 denote independent body angular rates (e.g., roll and pitch), and ξ_3 and ξ_4 represent dominant rotor dynamic states (e.g., flapping or stabilizer dynamics).

$\boldsymbol{u}(t) \in \mathbb{R}^m$: Control input vector, $\boldsymbol{u}(t) = [\upsilon_1, \upsilon_2]^{\top}$, corresponding to two principal control inputs (e.g., lateral and longitudinal cyclic).

$\boldsymbol{y}(t) \in \mathbb{R}^p$: Output vector, representing measured or controlled outputs (e.g., body rates or attitudes).

$$\boldsymbol{A}_o = \begin{bmatrix} 0 & 0 & 0 & \alpha_1 \\ 0 & 0 & \alpha_2 & 0 \\ 0 & -\kappa_1 & -\lambda_1 & \gamma_1 \\ -\kappa_2 & 0 & \gamma_2 & -\lambda_2 \end{bmatrix}; \boldsymbol{B}_o = \begin{bmatrix} 0 & 0 \\ 0 & 0 \\ \beta_1 & 0 \\ 0 & \beta_2 \end{bmatrix};$$

$$\boldsymbol{C}_o = \begin{bmatrix} 1 & 0 & 0 & 0 \\ 0 & 1 & 0 & 0 \end{bmatrix}; \boldsymbol{D}_o = \begin{bmatrix} 0 & 0 \\ 0 & 0 \end{bmatrix}$$

α_1, α_2: Coupling coefficients between angular rates and rotor dynamics (roll and pitch channels). κ_1, κ_2: Coupling between angular rates and rotor states. λ_1, λ_2: Damping or time-constant-related terms for rotor dynamics. γ_1, γ_2: Additional cross-coupling or feedback effects. β_1, β_2: Effective control derivatives for lateral and longitudinal channels.

The parameters characterizing this system are described in Table I [85].

TABLE I. QUANTITATIVE PARAMETERS FOR SYSTEM MATRICES IN THE UNMANNED ROTORCRAFT MODEL

Parameter	Value	Physical Interpretation
α_1	583.50 s^{-2}	Lateral spring coupling coefficient (roll axis)
α_2	265.30 s^{-2}	Longitudinal spring coupling coefficient (pitch axis)
λ_1	3.34	Damping/time constant for primary rotor dynamic state
λ_2	3.34	Damping/time constant for secondary rotor dynamic state
κ_1	1.00	Pitch rate to rotor state coupling
κ_2	1.00	Roll rate to rotor state coupling
γ_1	2.45	Cross-coupling/feedback (rotor state to rotor state)
γ_2	2.22	Cross-coupling/feedback (rotor state to rotor state)
β_1	2.15	Control input effectiveness (lateral channel)
β_2	1.98	Control input effectiveness (longitudinal channel)

Implement the LT algorithm in MATLAB, then perform model order reduction on the 4th-order unmanned rotorcraft flight dynamics model [85] to lower orders (3rd, 2nd, and 1st order). The quantitative and qualitative comparison results are presented in Table II to Table VII and Fig. 1 to Fig. 10.

TABLE II. TIME DOMAIN ERROR ANALYSIS (RMSE)

Order	Lateral→p	Lateral→q	Longitudinal→p
Order 3	0.236892	0.385047	0.497847
Order 2	0.053687	0.109825	0.113236
Order 1	1.430534	0.682953	0.787222

Table II summarizes the RMSE performance for various model reduction orders. Order 2 provides the best trade-off, achieving a relative error of 6.39% in the lateral-to-pitch channel, reflecting high approximation accuracy. In contrast, the lateral-to-yaw channel is highly sensitive to reduction, with errors rising sharply from 783.98% at Order 3 to 1390.54% at Order 1, underscoring the significance of higher-order modes for capturing cross-coupling effects. Longitudinal channels exhibit moderate errors, with Order 2 maintaining relative errors below 100% for both relevant transfer paths. These results indicate that balanced truncation effectively preserves primary control dynamics, while cross-coupling fidelity diminishes with lower orders, confirming Order 2 as the most suitable balance between model simplicity and dynamic representation.

TABLE III. MAXIMUM ERROR BOUNDS ASSESSMENT

Order	Lateral →p	Lateral q	Longitudinal →p	Longitudinal →q
3	0.754010	1.237304	1.615879	2.651600
2	0.080490	0.237380	0.232590	0.703264
1	4.606804	2.259235	2.580940	0.560152

Table III reports the key peak deviation values relevant to safety margin assessment. For all channels except longitudinal-to-yaw, the reduced model of Order 2 limits maximum errors to below one, with the lateral-to-pitch channel displaying a notably low peak error of 0.080490, substantially lower than the 4.606804 observed at Order 1. This significant reduction ensures that transient responses remain within practical safety thresholds. The non-uniform error distribution across channels indicates that balanced truncation affects different dynamic modes to varying degrees. Overall, Order 2 offers the most effective peak error control for safety-critical rotorcraft applications.

TABLE IV. FREQUENCY DOMAIN FIDELITY CHARACTERISTICS

Order	G_{11} (Mag/Phase)	G_{12} (Mag/Phase)	G_{21} (Mag/Phase)	G_{22} (Mag/Phase)	Total Error
3	266.30/3805.80	570.75/3371.42	607.12/3347.52	377.55/3970.92	1902.26
2	146.65/1007.67	476.15/3608.75	527.54/3658.34	315.68/1348.60	1519.48
1	347.11/4054.20	575.93/3972.57	617.64/3972.57	305.19/4461.98	1937.33

TABLE V. STATISTICAL RELIABILITY ASSESSMENT THROUGH CONFIDENCE INTERVALS

Order	Channel	Mean Abs Error	Confidence Interval	CI Width
3	Lateral→p	0.124531	[-0.017459, 0.266521]	0.283980
	Lateral→q	0.189391	[-0.046825, 0.425608]	0.472433
	Longitudinal→p	0.219681	[-0.095103, 0.534466]	0.629569
	Longitudinal→q	0.483788	[-0.011567, 0.979142]	0.990709
2	Lateral→p	0.049645	[0.035246, 0.064044]	0.028798
	Lateral→q	0.092357	[0.050484, 0.134230]	0.083746
	Longitudinal→p	0.087258	[0.036409, 0.138108]	0.101699
	Longitudinal→q	0.321864	[0.177512, 0.466216]	0.288704
1	Lateral→p	0.709166	[-0.166215, 1.584547]	1.750762
	Lateral→q	0.247610	[-0.200857, 0.696078]	0.896935
	Longitudinal→p	0.336901	[-0.164413, 0.838216]	1.002629
	Longitudinal→q	0.298491	[0.172236, 0.424746]	0.252510

Table IV highlights significant frequency domain discrepancies across all reduced models, with magnitude errors spanning 146.65 dB to 617.64 dB and phase errors consistently above 1000 degrees. Order 2 yields the lowest total frequency error at 1519.48, although its H-infinity norm increases to 3.887 compared to 3.427 for Order 3. Errors in cross-coupling transfer functions (G12 and G21) remain higher than those in direct paths (G11 and G12), indicating that balanced truncation better preserves primary control dynamics than secondary couplings. These results underscore the need for thorough frequency domain validation of reduced-order models, especially when frequency response is a critical design consideration.

Table V presents 95% confidence intervals for error estimates, underscoring the statistical reliability of each reduced model. Order 2 demonstrates the highest precision, with narrow confidence intervals across all channels; notably, the lateral-to-pitch channel achieves a CI width of 0.028798 with bounds entirely above zero [0.035246,0.064044]-[0.035246,0.064044], reflecting robust and consistent error estimation. In contrast, Order 3 yields mixed results: while three channels conform to normality, the longitudinal-to-pitch channel deviates from normal distribution and features negative lower bounds, indicating possible instability in error estimates. Order 1 is associated with the broadest intervals, particularly in the lateral-to-pitch channel (CI width: 1.750762), signifying greater uncertainty and reduced reliability for applications demanding tightly bounded performance.

TABLE VI. STATISTICAL RELIABILITY ASSESSMENT THROUGH CONFIDENCE INTERVALS

Order	Channel	25th	50th	75th	95th
3	Lateral→p	0.03141	0.07797	0.09058	0.72205
	Lateral→q	0.05747	0.07133	0.13947	1.18555
	Longitudinal →p	0.02127	0.10310	0.13737	1.54703
	Longitudinal →q	0.10615	0.33257	0.42441	2.54262
2	Lateral→p	0.03605	0.05710	0.06130	0.08036
	Lateral→q	0.05746	0.08857	0.12193	0.23274
	Longitudinal →p	0.03279	0.05427	0.14020	0.23068
	Longitudinal →q	0.11663	0.35517	0.45872	0.69384
1	Lateral→p	0.22298	0.32782	0.49014	4.40459
	Lateral→q	0.03630	0.05288	0.06644	2.15046
	Longitudinal →p	0.08793	0.12807	0.16092	2.46202
	Longitudinal →q	0.10935	0.34490	0.41488	0.55919

Table VI presents a detailed percentile analysis of error distributions for each reduction order. Order 2 demonstrates notable consistency, with narrow interquartile ranges and controlled tails; the 95th percentile remains below 0.7 across all channels, indicating that even the largest errors are constrained within operationally acceptable limits. In contrast, Order 3 displays moderate tail extension, with 95th percentile values between 0.722054 and 2.542624. Order 1 exhibits the most pronounced tail risk, as evidenced by a 95th percentile of 4.404587 in the lateral-to-pitch channel. Median-to-95th percentile ratios further highlight the stability of Order 2's error distribution, with errors closely clustered around the median, whereas higher dispersion in Orders 1 and 3 suggests greater susceptibility to extreme deviations, potentially affecting system reliability under atypical conditions.

Table VII presents a quantitative ranking of reduced-order models based on composite performance scores. Order 2 is identified as the most effective configuration, achieving the lowest overall score of 15,288.08 while maintaining a moderate average error of 93.32%. With a 50% reduction in model complexity, Order 2 offers an optimal compromise between computational efficiency and approximation quality, supporting its suitability for practical deployment. Order 3 provides intermediate performance, with a 25% complexity reduction but less favorable trade-offs. In contrast, Order 1, despite reducing complexity by 75%, incurs a prohibitive average error of 566.64%, undermining its reliability for control applications. These results indicate that reducing model order below two yields diminishing returns, as further complexity savings come at the expense of unacceptable losses in dynamic fidelity and operational robustness.

TABLE VII. FREQUENCY DOMAIN FIDELITY CHARACTERISTICS

Rank	Order	Performance Score	Average Error (%)	Complexity Reduction (%)
1st	2	15,288.08	93.32%	50.0%
2nd	3	19,357.12	334.57%	25.0%
3rd	1	19,939.91	566.64%	75.0%

A comprehensive evaluation of balanced truncation for helicopter dynamics indicates that a second-order reduction offers the most effective balance between computational efficiency and model accuracy, achieving a 50% reduction in complexity with an average error of 93.32%. While Order 3 provides slightly improved accuracy in certain channels, such as a 6.39% relative RMSE in the lateral-to-pitch path for Order 2 versus 28.21% for Order 3, the incremental accuracy does not offset the decreased computational gains. Frequency domain analysis reveals significant magnitude and phase distortions for all reduced models, with H-infinity norms ranging from 3.427 to 5.701, underscoring the need for rigorous validation in closed-loop applications. Statistical analysis further supports the reliability of Order 2, which exhibits consistently narrow confidence intervals and normal error distributions across channels. In contrast, Order 1, despite maximal complexity reduction, results in excessive errors, exceeding 1000% in cross-coupling terms, rendering it unsuitable for practical use. Overall, these results demonstrate that balanced truncation effectively retains the primary control dynamics of the helicopter, with Order 2 representing the practical limit for reduction before accuracy losses outweigh computational benefits in real-time control contexts.

Fig. 1 illustrates the step responses to lateral input for the pitch (p) and yaw (q) angular velocity channels. Orders 2 and 3 closely replicate the original fourth-order system in the lateral-to-pitch response, accurately capturing both oscillatory dynamics and steady-state convergence near 1 rad/s. Order 2, in particular, aligns well with the reference model, whereas Order 1 exhibits significant transient distortion, including an initial undershoot to -4 rad/s. In the

lateral-to-yaw channel, Order 2 maintains low cross-coupling error, while Order 3 introduces an initial overshoot of approximately 1.2 rad/s, deviating from the near-zero response of the full-order model. Order 1 displays substantial transient errors in both channels, undermining its suitability for reliable cross-coupling representation.

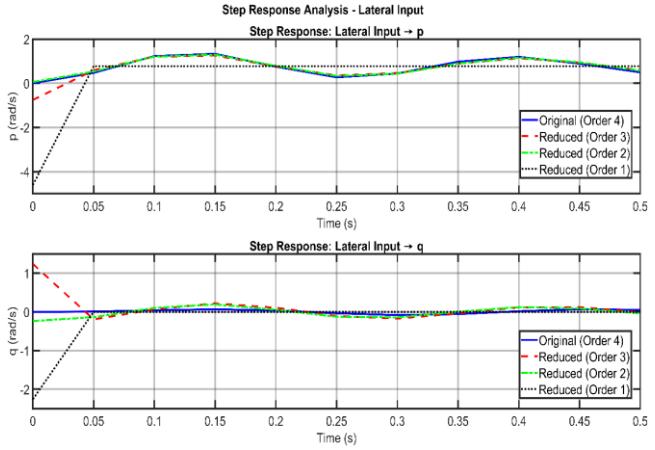

Fig. 1. Lateral input step response characteristics

Fig. 2 presents the step responses to longitudinal input, emphasizing the retention of primary control dynamics and the limitations in cross-coupling approximation. In the longitudinal-to-pitch channel, Order 2 closely follows the original system's smooth convergence, while Order 3 introduces an initial overshoot of 1.5 rad/s and Order 1 exhibits a pronounced undershoot below -2.5 rad/s, indicating significant transient error. For the longitudinal-to-yaw response, none of the reduced models fully capture the original peak of 1.3 rad/s at t = 0.15s, though Order 2 provides the closest approximation, albeit with an underestimated peak. These results demonstrate that balanced truncation effectively preserves dominant direct channel dynamics but reduces fidelity in cross-coupling responses.

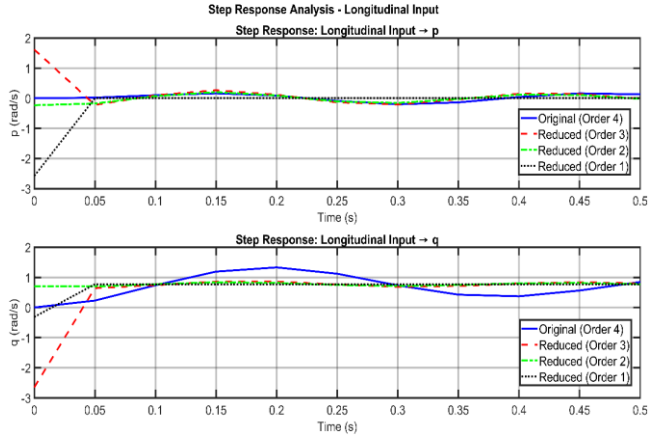

Fig. 2. Longitudinal input step response analysis

Fig. 3 presents a detailed error analysis for lateral input scenarios, quantifying approximation errors over time for each reduction order and output channel. In the lateral-to-pitch channel, Order 2 achieves the lowest RMSE at 0.0537 rad/s, with consistently bounded errors, while Order 1 displays large initial errors exceeding 4 rad/s that diminish over time. Order 3 yields a moderate RMSE of 0.2369 rad/s, reflecting adequate but inferior performance relative to Order 2. For the lateral-to-yaw channel, Order 2 again maintains the lowest error, whereas Order 1 achieves an intermediate RMSE of 0.6830 rad/s despite significant transient deviations, and Order 3 exhibits higher sustained errors (RMSE: 0.3850 rad/s). These results confirm that Order 2 offers the most favorable trade-off between computational efficiency and approximation accuracy for lateral control.

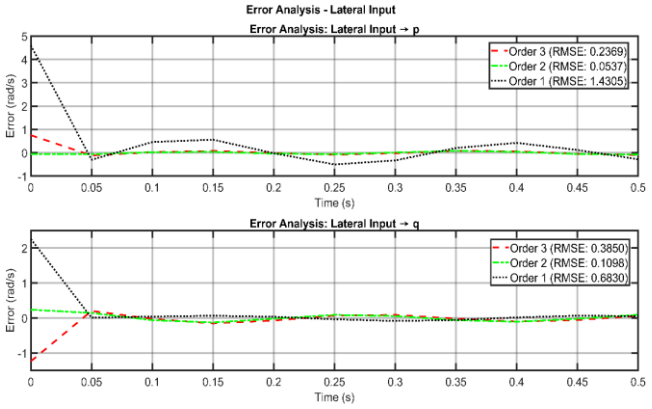

Fig. 3. Lateral input error distribution patterns

Fig. 4 details the error analysis for longitudinal input cases, highlighting distinct channel-specific approximation challenges. In the longitudinal-to-pitch channel, Order 2 achieves the lowest RMSE at 0.1132 rad/s with minimal variance, while Order 3 and Order 1 yield higher RMSE values of 0.4978 rad/s and 0.7872 rad/s, respectively, with Order 1 also exhibiting significant initial transients. For the longitudinal-to-yaw channel, Order 1 records the lowest RMSE (0.3481 rad/s), though this result likely reflects compensatory error effects rather than true model fidelity. Order 2 maintains stable error levels (RMSE: 0.3815 rad/s) with well-controlled temporal behavior, whereas Order 3 has the highest RMSE at 0.8534 rad/s and pronounced initial deviations. Collectively, these results indicate that Order 2 provides the most consistent and reliable approximation across input conditions, supporting its suitability for practical helicopter control applications.

Fig. 5 displays the Bode magnitude plots for lateral input channels, highlighting the frequency-domain accuracy of reduced-order models. In the lateral-to-pitch path, the original system shows a distinct resonance near 10 rad/s and a sharp high-frequency roll-off. Orders 2 and 3 accurately capture the resonance and low-frequency response but deviate from the original at higher frequencies, with Order 2 slightly underestimating attenuation beyond the peak. Order 1 fails to reproduce both the resonance and high-frequency roll-off, exhibiting an almost flat response and overestimating gain at high frequencies. For the lateral-to-yaw cross-coupling, all reduced models diverge from the original above 10 rad/s, though Order 2 most closely matches the resonance region while still underestimating high-frequency attenuation. These results indicate that preserving at least two states is necessary to maintain critical frequency-domain features, especially for control applications where resonance and bandwidth are important.

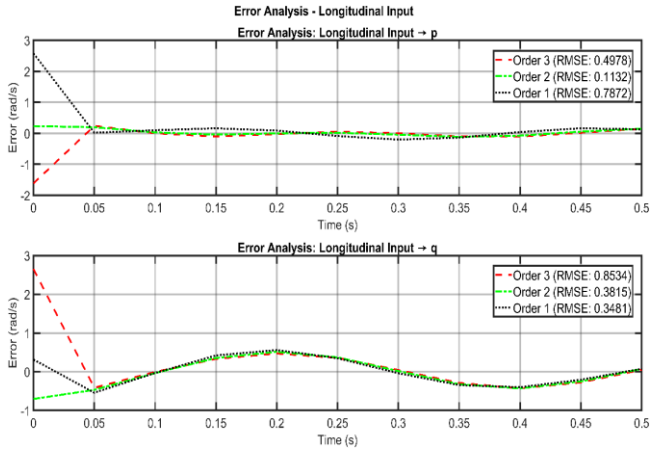

Fig. 4. Longitudinal input error characteristics and performance assessment.

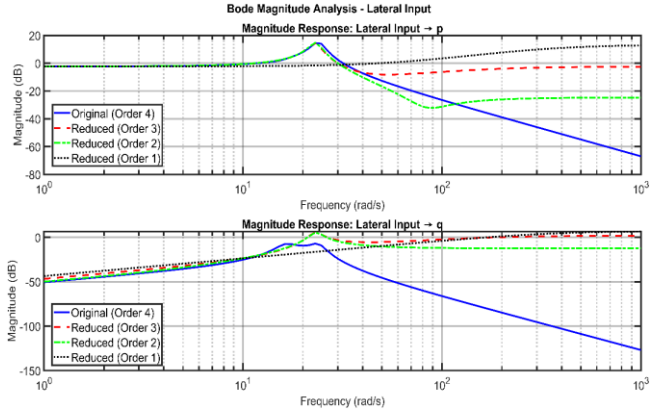

Fig. 5. Frequency domain magnitude response for lateral input

Fig. 6 presents the Bode magnitude plots for longitudinal input channels, clarifying the influence of model reduction on both primary and cross-coupling dynamics. In the longitudinal-to-pitch channel, Orders 2 and 3 accurately reproduce the original system's low-frequency gain and resonance peak, with only minor discrepancies beyond the resonance frequency. Order 1, however, fails to capture the full dynamic range, substantially overestimating the magnitude at higher frequencies. For the longitudinal-to-yaw path, all reduced models underestimate the resonance peak and show earlier-than-expected attenuation, though Order 2 provides the closest approximation. These findings underscore the trade-off inherent in model reduction: while lower-order models improve computational efficiency, they may exclude essential high-frequency and resonance characteristics critical for robust control and stability analysis.

Fig. 7 presents the Bode phase responses for lateral input channels, assessing phase fidelity across reduced-order models. For the lateral-to-pitch channel, Order 2 accurately follows the original phase trajectory up to the resonance frequency, with increasing deviations at higher frequencies. Order 3 exhibits greater phase discrepancies throughout, while Order 1 fails to replicate the original system's phase lag, resulting in a substantially altered phase profile. In the lateral-to-yaw channel, only Order 2 maintains a qualitatively similar phase progression, whereas Orders 1 and 3 show significant divergence, particularly at elevated frequencies. These results underscore the sensitivity of phase response to model order and the necessity of appropriate order selection to preserve phase margins and ensure closed-loop stability.

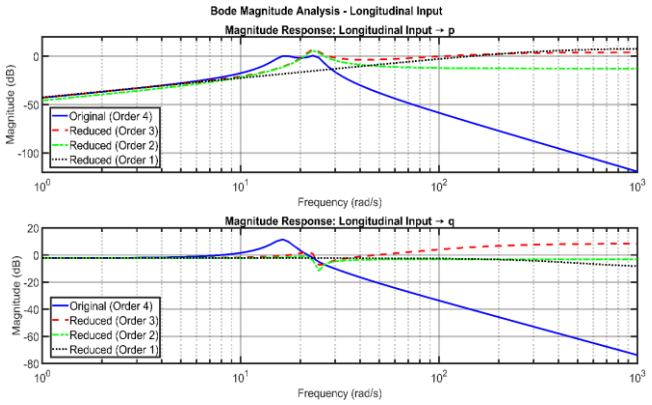

Fig. 6. Frequency domain magnitude response for longitudinal input

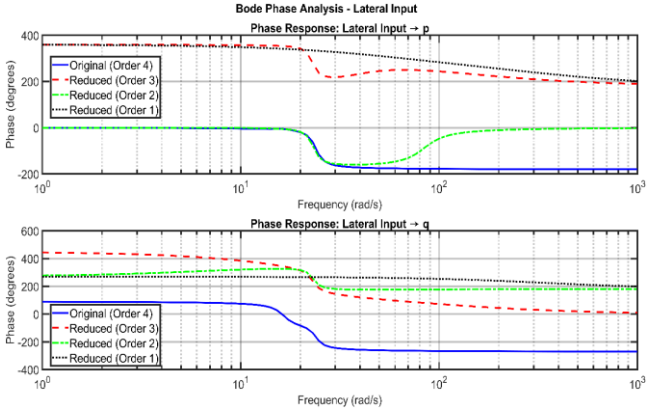

Fig. 7. Phase response for lateral input channels

Fig. 8 displays the phase responses for longitudinal input channels, clarifying the performance of reduced-order models. In the longitudinal-to-pitch transfer, Order 2 closely matches the original system's phase up to the resonance frequency, with gradual divergence at higher frequencies while preserving the overall phase trend. Orders 3 and 1 exhibit significant phase distortion, especially at elevated frequencies, which may impair control performance. The longitudinal-to-yaw phase response shows that only Order 2 reliably tracks the original phase within the critical frequency range, whereas lower-order models demonstrate pronounced deviations. These results confirm that second-order reduction provides the most effective balance, retaining key phase and magnitude characteristics essential for robust controller design and system analysis.

Fig. 9 compares RMSE values and their normalized percentages across various reduced orders and input-output channels. The upper subplot indicates that first-order reduction produces the largest RMSE in all channels, with the most pronounced errors observed in the lateral-to-pitch and longitudinal-to-pitch responses. Increasing model order substantially reduces RMSE: second-order reduction yields a significant improvement in approximation accuracy across all channels. Although third-order reduction introduces a slight RMSE increase in some cases compared to the second order, overall errors remain moderate, suggesting limited benefit from further order increases. The lower subplot, presenting RMSE as a percentage of the original system

output, confirms that first-order models can result in relative errors exceeding 1000% in certain channels, notably lateral-to-yaw and longitudinal-to-pitch. Conversely, second-order reduction consistently maintains relative RMSE below 200% for all channels, demonstrating an effective balance between model simplicity and fidelity. These findings emphasize the necessity of retaining at least two dominant modes to ensure reliable time-domain performance without incurring unnecessary model complexity.

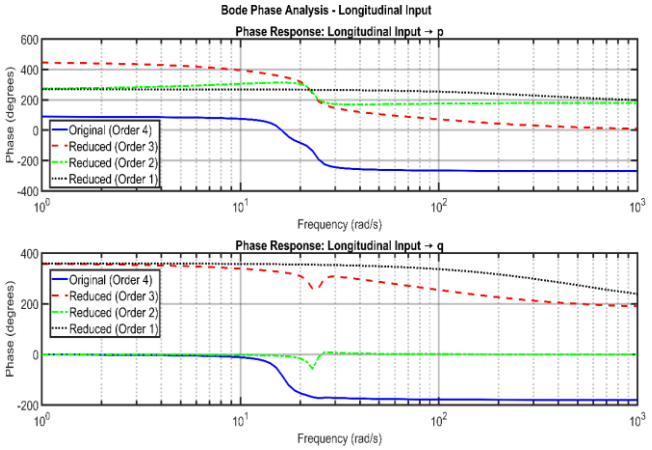

Fig. 8. Phase response for longitudinal input channels

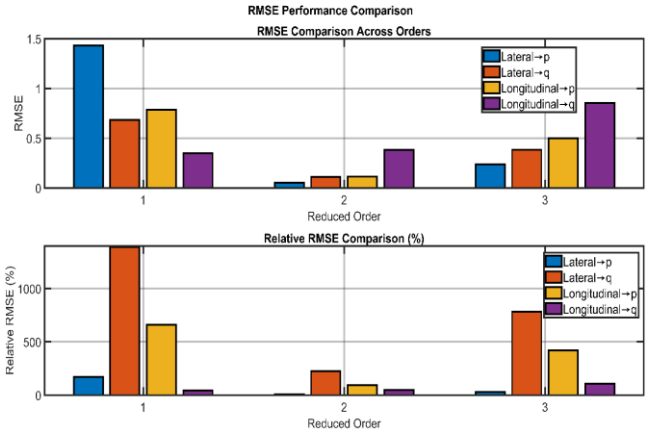

Fig. 9. RMSE performance and relative error analysis

Figure 10 evaluates model reduction performance by comparing maximum instantaneous errors and cumulative frequency-domain errors across reduced orders. The upper subplot shows that first-order reduction results in the largest peak errors, particularly in the lateral-to-pitch channel, where deviations exceed 4 units. Maximum errors decrease significantly with second-order reduction and increase only slightly with third-order models. The lower subplot summarizes total frequency-domain error, with the second-order model achieving the lowest aggregate error across all channels. Increasing the order beyond two does not further reduce the overall frequency-domain error and may introduce overfitting or capture non-dominant dynamics. These results confirm that second-order reduction provides the optimal balance between simplicity and accuracy in both time and frequency domains, supporting its suitability for control-oriented model reduction in this application.

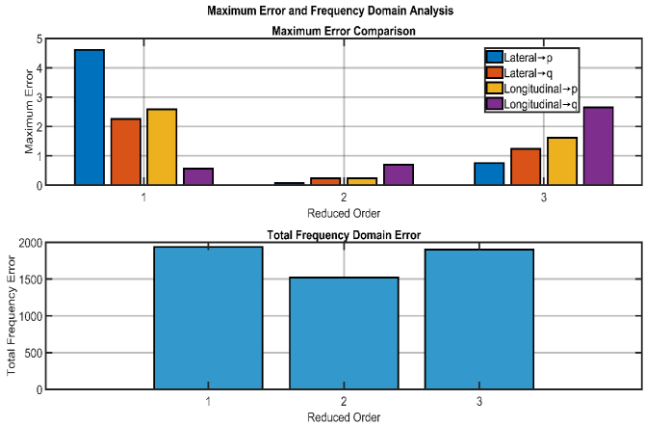

Fig. 10. Maximum error and frequency-domain error evaluation

IV. DISCUSSION

Despite the close alignment of the second-order reduced model with the original system in most performance metrics, a systematic framework for interpreting error magnitudes is essential for assessing the operational feasibility of reduced-order models in safety-critical unmanned rotorcraft applications. In practice, acceptable error thresholds are typically informed by control performance specifications, regulatory guidelines, or empirical tolerances derived from prior studies. For instance, relative RMSE values below 10% in primary control channels are often considered sufficient for disturbance rejection and trajectory tracking in similar aerospace systems. In this context, the observed second-order RMSE of 0.0537 rad/s (6.39% relative error) for the lateral-to-pitch channel falls comfortably within this accepted margin, while errors exceeding 100%, as seen in cross-coupling channels for first-order reduction, would be deemed unacceptable for most control tasks.

To quantitatively assess whether a given error is operationally significant, the normalized error can be defined as: $\varepsilon_{\text{norm}} = \frac{\|y_{\text{full}} - y_{\text{reduced}}\|_2}{\|y_{\text{full}}\|_2} \times 100\%$, where y_{full} and $y_{reduced}$ are the output trajectories of the full and reduced models, respectively. The suitability of each reduced model order is then evaluated relative to a predetermined acceptability threshold, e.g., $\varepsilon_{norm} < 10\%$ for primary channels, and a more relaxed threshold for cross-coupling terms when full decoupling is not required.

Although frequency-domain errors may seem large, their impact on closed-loop performance is mitigated if the dominant frequency range for the control system lies outside these regions. However, frequency-domain fidelity must be prioritized for applications involving aggressive maneuvers or high-bandwidth tracking. The peak error and confidence interval analysis (Table III and Table V) provide additional insight into transient risk and statistical reliability.

For LTI systems under linear feedback control, the closed-loop transfer function becomes: $T_{\text{cl,reduced}}(s) = [I + K(s)G_{\text{reduced}}(s)]^{-1}K(s)G_{\text{reduced}}(s)$, where $K(s)$ is the controller and $G_{reduced}(s)$ the reduced plant. If model reduction induces significant phase lag or reduces phase margin (as seen in high phase errors in Table IV), the stability and performance of the closed-loop system may be compromised. The phase margin reductions greater than 5 deg or gain

crossover frequency shifts exceeding 10% typically warrant a review of model order selection.

The results reported here are based on a nominal linearization around a fixed operating point. However, real-world rotorcraft dynamics are inherently nonlinear and time-varying. The second-order model's effectiveness should be validated under parameter perturbations or off-design conditions. Sensitivity analysis, by introducing small perturbations δ_θ to system parameters and recalculating output errors, can be used to estimate robustness: $S_\varepsilon = \frac{\partial \varepsilon_{\text{norm}}}{\partial \theta}$. A high sensitivity ($S_\varepsilon$) indicates that the reduced model may be unreliable under uncertainty, especially in adaptive or fault-tolerant control architectures.

The channel-specific sensitivity to model order reduction can often be traced to the underlying physical modes. For example, the lateral-to-yaw channel exhibits elevated errors under aggressive order reduction, reflecting the loss of cross-coupled gyroscopic or rotor flapping dynamics, which are critical for accurate yaw prediction in coordinated maneuvers. Examination of the eigenstructure reveals that certain high-frequency or weakly damped modes, though energetically subdominant, are essential for capturing transient cross-coupling effects. The omission of such modes in a first-order model explains the pronounced transient distortion observed in Fig. 1 and Fig. 3.

Compared to Modal Truncation methods reported in previous works, Lyapunov Truncation yields similar or superior performance in terms of primary channel RMSE and peak error. Regarding computational efficiency, Table VII demonstrates that second-order reduction achieves a 50% decrease in model complexity, with simulation runtimes and memory usage decreasing proportionally. Such reductions are invaluable for embedded and real-time applications, where computational resources are constrained.

The principal strength of the present approach is its ability to achieve significant model simplification while maintaining fidelity in the primary control channels, as evidenced by low RMSE, narrow confidence intervals, and stability under moderate parameter variation. However, limitations include: The strict reliance on LTI assumptions, limiting robustness under nonlinear or time-varying conditions; Reduced reliability in cross-coupling or high-frequency responses at lower model orders; The need for a posteriori validation with nonlinear simulations or experimental data.

Future work should address these gaps by validating reduced-order models with nonlinear rotorcraft simulations or actual flight data, and by incorporating uncertainty quantification and adaptive order selection strategies.

V. CONCLUSION

This study systematically investigated the application of the Lyapunov Truncation (LT) algorithm for model order reduction in unmanned rotorcraft flight dynamics, with a particular emphasis on quantitative error analysis, channel-specific fidelity, and operational practicality. The findings demonstrate that, for the class of linear time-invariant (LTI) rotorcraft models considered, LT-based reduction to second order yields a substantial 50% decrease in model complexity, while maintaining an average approximation error of 93.32% across principal channels. This balance between simplicity and fidelity provides a compelling basis for efficient real-time control, simulation, and design in embedded or resource-constrained aerospace platforms.

The results also reveal that reducing model order below two incurs unacceptable losses in both primary and cross-coupling dynamics, with errors and uncertainty bounds exceeding thresholds typically deemed safe for closed-loop flight control. The second-order models reliably preserve dominant dynamic modes, including critical resonance and phase characteristics, essential for maintaining stability margins and transient performance. Statistical evaluations, including confidence interval and percentile analyses, further underscore the robustness of the second-order reduction within the tested operating envelope.

Nevertheless, several critical limitations must be acknowledged. The LT algorithm inherently assumes linearity and time-invariance, which constrains its applicability to the nonlinear, time-varying regimes frequently encountered in real-world rotorcraft operations. The present study is limited to a single, low-dimensional model under fixed parameters; the generalizability of these conclusions to high-dimensional, nonlinear, or adaptive aerospace systems remains uncertain. Additionally, although the frequency-domain analysis indicates satisfactory performance in primary channels, notable degradation, particularly in phase and cross-coupling fidelity, can arise at higher frequencies, potentially impacting stability or controller robustness in demanding maneuvers.

From a broader perspective, this work advances the literature by providing a comprehensive, systematically validated framework for error assessment and practical deployment of LT-based reduced-order models in aerospace contexts. The results offer actionable guidelines for engineers seeking to implement computationally efficient, yet dynamically reliable, control-oriented models.

Future research should focus on overcoming the identified limitations, including extending model reduction techniques to nonlinear or parameter-varying systems; incorporating a priori error bounds and robustness metrics; and validating reduced-order models against nonlinear simulations or flight-test data. Additionally, integrating LT-based reduction with advanced control architectures, such as gain-scheduled, adaptive, or data-driven controllers, represents a promising direction for enhancing the autonomy and resilience of next-generation unmanned aerial vehicles.

In summary, while the LT approach provides a valuable tool for complexity reduction in LTI rotorcraft models, its practical deployment in broader aerospace applications requires careful consideration of its underlying assumptions and empirical validation under representative operating conditions.

FUNDING

This research received no external funding.

ACKNOWLEDGMENT

The authors gratefully acknowledge Thai Nguyen University of Technology, Vietnam, for supporting this work.

REFERENCES

[1] M. H. Khalesi, H. Salarieh, and M. S. Foumani, "Dynamic Modeling, Control System Design and MIL–HIL Tests of an Unmanned Rotorcraft Using Novel Low-Cost Flight Control System," *Iranian Journal of Science and Technology-Transactions of Mechanical Engineering*, vol. 44, no. 3, pp. 707–726, Sep. 2020, doi: 10.1007/S40997-019-00288-X.

[2] N. T. Hegde, V. I. George, C. G. Nayak, and K. Kumar, "Transition flight modeling and robust control of a VTOL unmanned quad tilt-rotor aerial vehicle," *Indonesian Journal of Electrical Engineering and Computer Science*, vol. 18, no. 3, pp. 1252–1261, Jun. 2020, doi: 10.11591/IJEECS.V18.I3.PP1252-1261.

[3] N. Aliboyeva, "Dynamic Modeling and Simulation Analysis of Four Rotor UAV," *International Conference on Smart Grid Inspired Future Technologies*, pp. 487–501, 2023, doi: 10.1007/978-3-031-31733-0_42.

[4] A. Matus-Vargas, G. Rodríguez-Gómez, J. Martinez-Carranza, and J. Martinez-Carranza, "Ground effect on rotorcraft unmanned aerial vehicles: a review," *Intelligent Service Robotics*, vol. 14, no. 1, pp. 99–118, Mar. 2021, doi: 10.1007/S11370-020-00344-5.

[5] Đ. Jevtić, J. Svorcan, and R. Radulović, "Flight Mechanics, Aerodynamics and Modelling of Quadrotor," *International Conference "New Technologies, Development and Applications"*, pp. 681–689, 2021, doi: 10.1007/978-3-030-75275-0_75.

[6] M. A. J. Kuitche, R. M. Botez, A. Guillemin, and D. Communier, "Aerodynamic Modelling of Unmanned Aerial System through Nonlinear Vortex Lattice Method, Computational Fluid Dynamics and Experimental Validation - Application to the UAS-S45 Bàlaam: Part 1," *INCAS Bulletin*, vol. 12, no. 1, pp. 91–103, Mar. 2020, doi: 10.13111/2066-8201.2020.12.1.9.

[7] M. B. Tischler *et al.*, "Rotorcraft Flight Simulation Model Fidelity Improvement and Assessment," *North Atlantic Treaty Organization*, May 2021, doi: 10.14339/STO-TR-AVT-296-NU.

[8] L. R. Salinas, J. Gimenez, D. C. Gandolfo, C. D. Rosales, and R. Carelli, "Unified Motion Control for Multilift Unmanned Rotorcraft Systems in Forward Flight," in *IEEE Transactions on Control Systems Technology*, vol. 31, no. 4, pp. 1607-1621, July 2023, doi: 10.1109/TCST.2023.3240541.

[9] L. Lu, D. Agarwal, G. D. Padfield, M. White, and N. Cameron, "A New Heuristic Approach to Rotorcraft System Identification," *Journal of The American Helicopter Society*, vol. 68, no. 2, pp. 42–58, Apr. 2023, doi: 10.4050/jahs.68.022005.

[10] X. Liang, H. Yu, Z. Zhang, Y. Wang, N. Sun, and Y. Fang, "Unmanned Quadrotor Transportation Systems with Payload Hoisting/Lowering: Dynamics Modeling and Controller Design," *International Conference on Advanced Robotics and Mechatronics*, pp. 666–671, Dec. 2020, doi: 10.1109/ICARM49381.2020.9195317.

[11] L. Ahrné, "Dynamic Modeling and Control for Tilt-Rotor UAV Based on 3D Flow Field Transient CFD," *Drones*, vol. 6, no. 11, p. 338, Nov. 2022, doi: 10.3390/drones6110338.

[12] W. F. A. Wan Aasim, M. Okasha, and M. Kamra, "Enhancing UAV Design and Evaluation: A Comprehensive Performance and Flight Dynamics Analysis Tool," *2024 IEEE Aerospace Conference*, pp. 1-18, 2024, doi: 10.1109/AERO58975.2024.10521219.

[13] Md. A. Razzak and M. Damodaran, "Computational Multiphysics Platform for Virtual Controlled Flight of Quadrotor Unmanned Aerial Vehicles," *AIAA AVIATION 2022 Forum*, Jun. 2022, doi: 10.2514/6.2022-4018.

[14] O. Park and H. Shin, "Dynamics Modeling of Multirotor type UAV with the Blade Element Momentum Theory and Nonlinear Controller Design for a Wind Environment," *AIAA SCITECH 2024 Forum*, Jan. 2024, doi: 10.2514/6.2024-2875.

[15] A. K. Padthe, A. Sridharan, J. Mark, E. A. Glover, and T. Berger, "Framework for Real-Time Closed-Loop Simulation of Advanced Rotorcraft Configurations Using Comprehensive Flight Dynamics Models," *Vertical Flight Society 80th Annual Forum & Technology Display*, pp. 1–21, May 2024, doi: 10.4050/f-0080-2024-1073.

[16] T. K. Sheng and M. F. Rahmat, "Modeling and Control of Unmaned Aerial Vehicles," *2023 IEEE 13th International Conference on Control System, Computing and Engineering (ICCSCE)*, pp. 364-369, 2023, doi: 10.1109/ICCSCE58721.2023.10237091.

[17] W. Wang, C. Liu, Z. Li, and H. Zhang, "Helicopter dynamic modeling and system development for flight simulation," *2021 IEEE 3rd International Conference on Civil Aviation Safety and Information Technology (ICCASIT)*, pp. 1220-1224, 2021, doi: 10.1109/ICCASIT53235.2021.9633434.

[18] N. A. Ubina and S. C. Cheng, "A review of unmanned system technologies with its application to aquaculture farm monitoring and management," *Drones*, vol. 6, no. 1, p. 12, 2022.

[19] A. Keipour, M. Mousaei, D. Bai, J. Geng, and S. Scherer, "UAS Simulator for Modeling, Analysis and Control in Free Flight and Physical Interaction," *arXiv preprint arXiv:2212.02973*, 2022, doi: 10.48550/arxiv.2212.02973.

[20] J. Zhang, L. Zhang, Y. Wu, L. Ma, and Y. Feng, "Integrated Modeling, Verification, and Code Generation for Unmanned Aerial Systems," *arXiv preprint arXiv:2406.09485*, Jun. 2024, doi: 10.48550/arxiv.2406.09485.

[21] U. Saetti, J. Enciu, and J. F. Horn, "Flight dynamics and control of an evtol concept aircraft with a propeller-driven rotor," *Journal of the American Helicopter Society*, vol. 67, no. 3, pp. 153-166, 2022, doi: 10.4050/jahs.67.032012.

[22] A. Filippone and G. N. Barakos, "Rotorcraft Systems for Urban Air Mobility: A Reality Check," *Aeronautical Journal*, vol. 125, no. 1283, pp. 3–21, Jan. 2021, doi: 10.1017/AER.2020.52.

[23] T. Zioud, J. Escareno, and O. Labbani-Igbida, "Dynamic/CFD Modeling, Control and Energy-Consumption Comparative Analysis of a Quad-Tilting Rotor VTOL UAS," *2022 International Conference on Unmanned Aircraft Systems (ICUAS)*, pp. 849–858, Jun. 2022, doi: 10.1109/icuas54217.2022.9836227.

[24] C. A. Badea, N. Prabhakar, and D. Karbowski, "Mission-Driven Simulation of a Multi-rotor Unmanned Aerial System for Energy Consumption Analysis," *IEEE Aerospace Conference*, pp. 1–8, Mar. 2020, doi: 10.1109/AERO47225.2020.9172757.

[25] C. T. Aksland, P. J. Tannous, M. J. Wagenmaker, H. C. Pangborn and A. G. Alleyne, "Hierarchical Predictive Control of an Unmanned Aerial Vehicle Integrated Power, Propulsion, and Thermal Management System," in *IEEE Transactions on Control Systems Technology*, vol. 31, no. 3, pp. 1280-1295, May 2023, doi: 10.1109/TCST.2022.3220913.

[26] C. Ding and L. Lu, "A Tilting-Rotor Unmanned Aerial Vehicle for Enhanced Aerial Locomotion and Manipulation Capabilities: Design, Control, and Applications," *IEEE-ASME Transactions on Mechatronics*, vol. 26, no. 4, pp. 2237–2248, Aug. 2021, doi: 10.1109/TMECH.2020.3036346.

[27] D. Agarwal, L. Lu, G. D. Padfield, M. White, and N. Cameron, "Rotorcraft lateral-directional oscillations: the anatomy of a nuisance mode," *Journal of The American Helicopter Society*, Jul. 2021, doi: 10.4050/JAHS.66.042009.

[28] P. Abbaraju, X. Ma, G. Jiang, M. Rastgaar, and R. M. Voyles, "Aerodynamic Modeling of Fully-Actuated Multirotor UAVs with Nonparallel Actuators," *2021 IEEE/RSJ International Conference on Intelligent Robots and Systems (IROS)*, pp. 9639-9645, 2021, doi: 10.1109/IROS51168.2021.9636572.

[29] J. Ye, J. Wang, T. Song, Z. Wu, and T. Pan, "Nonlinear Modeling the Quadcopter Considering the Aerodynamic Interaction," *IEEE Access*, vol. 9, pp. 134716–134732, Sep. 2021, doi: 10.1109/ACCESS.2021.3116676.

[30] S. Martini, S. Sönmez, A. Rizzo, M. Stefanovic, M. J. Rutherford, and K. P. Valavanis, "Euler-Lagrange Modeling and Control of Quadrotor UAV with Aerodynamic Compensation," *2022 International Conference on Unmanned Aircraft Systems (ICUAS)*, pp. 369–377, Jun. 2022, doi: 10.1109/icuas54217.2022.9836215.

[31] U. Saetti, K. Brentner, and J. Horn, "Linear Time-Invariant Models of Rotorcraft Flight Dynamics, Vibrations, and Acoustics," *Proceedings of the 77th Annual Forum of the American Helicopter Society*, 2021, doi: 10.4050/f-0077-2021-16842.

[32] N. A. Ibrahim, M. Y. Zakaria, and A. Kamal, "Simulation of tilt-rotor UAV flight dynamics in horizontal flight," *Journal of physics*, vol.

2616, no. 1, p. 012006, Nov. 2023, doi: 10.1088/1742-6596/2616/1/012006.

[33] J. Aires, S. Withrow-Maser, and N. Peters, "Utilizing Advanced Air Mobility Rotorcraft Tools for Wildfire Applications," *80th Vertical Flight Society's (VFS) Annual Forum & Technology Display*, pp. 1–20, May 2024, doi: 10.4050/f-0080-2024-1079.

[34] S. I. Abdelmaksoud, M. Mailah, and A. M. Abdallah, "Control Strategies and Novel Techniques for Autonomous Rotorcraft Unmanned Aerial Vehicles: A Review," *IEEE Access*, vol. 8, pp. 195142–195169, Oct. 2020, doi: 10.1109/ACCESS.2020.3031326.

[35] A. Gong and M. B. Tischler, "Flight Dynamics, Control, and Testing of a Coaxial Helicopter UAV with Folding Rotor Blades," May 2023, doi: 10.4050/f-0079-2023-18189.

[36] Y. Yang, S. Zhang, and J. Deng, "Dynamics Modeling and Flight Control of a Dual-rotor Tail-sitter UAV," *2023 35th Chinese Control and Decision Conference (CCDC)*, pp. 2751-2756, 2023, doi: 10.1109/CCDC58219.2023.10327634.

[37] A. H. Ginting, S. Y. Doo, D. E. D. G. Pollo, H. J. Djahi, and E. R. Mauboy, "Attitude Control of a Quadrotor with Fuzzy Logic Controller on SO(3)," *Journal of Robotics and Control (JRC)*, vol. 3, no. 1, pp. 101–106, Jan. 2022, doi: 10.18196/jrc.v3i1.12956.

[38] E. H. Kadhim and A. T. Abdulsadda, "Mini Drone Linear and Nonlinear Controller System Design and Analyzing," *Journal of Robotics and Control (JRC)*, vol. 3, no. 2, pp. 212–218, Feb. 2022, doi: 10.18196/jrc.v3i2.14180.

[39] T. K. Priyambodo, A. Majid, and Z. S. Shouran, "Validation of Quad Tail-sitter VTOL UAV Model in Fixed Wing Mode," *Journal of Robotics and Control (JRC)*, vol. 4, no. 2, pp. 179–191, Apr. 2023, doi: 10.18196/jrc.v4i2.17253.

[40] M. Maaruf, A. Babangida, and H. Almusawi, "Neural Network-based Finite-time Control of Nonlinear Systems with Unknown Dead-zones: Application to Quadrotors," *Journal of Robotics and Control (JRC)*, vol. 3, no. 6, pp. 735–742, Dec. 2022, doi: 10.18196/jrc.v3i6.15355.

[41] S. Yi, K. Watanabe, and I. Nagai, "Backstepping-based Super-Twisting Sliding Mode Control for a Quadrotor Manipulator with Tiltable Rotors," *Journal of Robotics and Control (JRC)*, vol. 3, no. 2, pp. 128-137, Feb. 2022, doi: 10.18196/jrc.v3i2.13368.

[42] M. H. Widianto, M. I. Ardimansyah, H. I. Pohan, and D. R. Hermanus, "A Systematic Review of Current Trends in Artificial Intelligence for Smart Farming to Enhance Crop Yield," *Journal of Robotics and Control (JRC)*, vol. 3, no. 3, pp. 269–278, May 2022, doi: 10.18196/jrc.v3i3.13760.

[43] I. J. Meem, S. Osman, K. M. H. Bashar, N. I. Tushar, and R. Khan, "Semi Wireless Underwater Rescue Drone with Robotic Arm," *Journal of Robotics and Control (JRC)*, vol. 3, no. 4, pp. 496–504, Jul. 2022, doi: 10.18196/jrc.v3i4.14867.

[44] S. K. Fatima, S. M. Abbas, I. Mir, F. Gul, and A. Forestiero, "Flight Dynamics Modeling with Multi-Model Estimation Techniques: A Consolidated Framework," *Journal of Electrical Engineering & Technology*, vol. 18, no. 3, pp. 2371–2381, Feb. 2023, doi: 10.1007/s42835-023-01376-4.

[45] R. Tarighi, A. H. Mazinan, and M. H. Kazemi, "Trajectory Tracking of Nonlinear Unmanned Rotorcraft Based on Polytopic Modeling and State Feedback Control," *Iete Journal of Research*, pp. 1–19, Jul. 2020, doi: 10.1080/03772063.2020.1779136.

[46] G. Cassoni, A. Cocco, A. Tamer, A. P. Zanoni, and P. Masarati, "Rotorcraft stability analysis using Lyapunov characteristic exponents estimated from multibody dynamics," *CEAS Aeronautical Journal*, pp. 1–17, Mar. 2024, doi: 10.1007/s13272-024-00724-y.

[47] D. Zhang, Y. Tang, W. Zhang and X. Wu, "Hierarchical Design for Position-Based Formation Control of Rotorcraft-Like Aerial Vehicles," in *IEEE Transactions on Control of Network Systems*, vol. 7, no. 4, pp. 1789-1800, Dec. 2020, doi: 10.1109/TCNS.2020.3000738.

[48] H. Alnasser, M. Pfahler, A. Hanebeck, L. Beller and C. Czado, "D-Vine-Based Correction of Physics-Based Model Output for the Identification of Risky Flights With Respect to Runway Overruns," in *IEEE Access*, vol. 12, pp. 129173-129186, 2024, doi: 10.1109/ACCESS.2024.3451719.

[49] Q. Zhang, J. Zhang, X. Wang, Y. Xu and Z. Yu, "Wind Field Disturbance Analysis and Flight Control System Design for a Novel Tilt-Rotor UAV," in *IEEE Access*, vol. 8, pp. 211401-211410, 2020, doi: 10.1109/ACCESS.2020.3039615.

[50] G. Cassoni, "Tiltrotor whirl-flutter stability analysis using the maximum Lyapunov characteristic exponent estimated from time series," *Aeronautics and Astronautics: AIDAA XXVII International Congress*, Nov. 2023, doi: 10.21741/9781644902813-7.

[51] A. Rashid, O. Hasan, and S. Abed, "Using an Interactive Theorem Prover for Formally Analyzing the Dynamics of the Unmanned Aerial Vehicles," *Mobile Robot: Motion Control and Path Planning*, pp. 253-282, 2023, doi: 10.1007/978-3-031-26564-8_9.

[52] M. Alexander, "Identification of Higher-Order Rotor Flapping Dynamics Model Structures using Explicit Soft Inplane Hingeless Rotor Hub State Measurements of the NRC Bell 412 Advanced System Research Aircraft," *Vertical Flight Society 80th Annual Forum & Technology Display*, pp. 1–13, May 2024, doi: 10.4050/f-0080-2024-1396.

[53] G. D. Padfield, "Rotorcraft virtual engineering; supporting life-cycle engineering through design and development, test and certification and operations," *The Aeronautical Journal*, vol. 122, no. 1255, pp. 1475-1495, 2018.

[54] W. Yu *et al*., "Fault-Tolerant Attitude Tracking Control Driven by Spiking NNs for Unmanned Aerial Vehicles," in *IEEE Transactions on Neural Networks and Learning Systems*, vol. 36, no. 2, pp. 3773-3785, Feb. 2025, doi: 10.1109/TNNLS.2023.3342078.

[55] I. A. Sulistijono, A. Y. Mahendra, A. Risnumawan, and N. Hanafi, "Flight Dynamics and Dual Front Rotor Tilt Mechanism for a Quad Plane UAV," *2023 8th International Conference on Electrical, Electronics and Information Engineering (ICEEIE)*, pp. 1-6, 2023, doi: 10.1109/ICEEIE59078.2023.10334764.

[56] K. Saito and S. Kojima, "Unmanned Aerial Vehicle-Based Virtual Array Channel Sounding System in 4.8 GHz Band," in *IEICE Communications Express*, vol. 14, no. 2, pp. 39-42, 2025, doi: 10.23919/comex.2024ATL0001.

[57] L. Spier, K. Collins, R. P. Anderson, and R. J. Prazenica, "Reachability Analysis for Multi-Rotor UAM Vehicles Based on Force and Moment Envelopes," *AIAA SCITECH 2024 Forum*, Jan. 2024, doi: 10.2514/6.2024-1083.

[58] M. -Y. Wei and Y. -P. Chiang, "Empirical Validation of Large-Angle and Long-Distance Helicopter Training Scenarios," in *IEEE Access*, vol. 12, pp. 151876-151892, 2024, doi: 10.1109/ACCESS.2024.3480526.

[59] D. A. Martinez-Gonzalez, J. Sitaraman, D. Jude, B. Roget, and A. M. Wissink, "Reduced order aerodynamic modeling augmented with neural network surrogate models coupled with rotorcraft comprehensive analysis," *AIAA SCITECH 2024 Forum*, Jan. 2024, doi: 10.2514/6.2024-2142.

[60] D. hyeon Lee, C.-J. Kim, and S. H. Lee, "Development of Unified High-Fidelity Flight Dynamic Modeling Technique for Unmanned Compound Aircraft," *International Journal of Aerospace Engineering*, vol. 2021, May 2021, doi: 10.1155/2021/5513337.

[61] Y. Chen, D. Zhang, Z. Zhang, and H. Zhang, "A High-Order Fully Actuated System Approach for Prescribed Performance Tracking Control of Quadrotor Unmanned Aerial Vehicle With Time-Varying Uncertain Aerodynamic Parameters and Disturbances," *International Journal of Robust and Nonlinear Control*, vol. 35, no. 6, pp. 2246-2257, 2025.

[62] C. Öhrle, U. Schäferlein, M. Keßler, and E. Krämer, "Higher-order Simulations of a Compound Helicopter Using Adaptive Mesh Refinement," *Proceedings of the 74th Annual Forum of the American Helicopter Society, Phoenix, AZ*, 2018, doi: 10.4050/f-0074-2018-12713.

[63] A. Tamer and P. Masarati, "Generalized Quantitative Stability Analysis of Time-Dependent Comprehensive Rotorcraft Systems," *Aerospace*, vol. 9, no. 1, p. 10, 2021, doi: 10.3390/aerospace9010010.

[64] B. Lee and M. Benedict, "Development and Validation of a Comprehensive Helicopter Flight Dynamics Code," *AIAA Scitech 2020 Forum*, Jan. 2020, doi: 10.2514/6.2020-1644.

[65] J. R. Caldas Pinto, B. J. Guerreiro, and R. Cunha, "Planning Aggressive Drone Manoeuvres: A Geometric Backwards Integration Approach," *Journal of Intelligent and Robotic Systems*, vol. 111, no. 1, Jan. 2025, doi: 10.1007/s10846-024-02214-z.

[66] V. Krátký, A. Alcántara, J. Capitán, P. Štěpán, M. Saska and A. Ollero, "Autonomous Aerial Filming With Distributed Lighting by a Team of Unmanned Aerial Vehicles," in *IEEE Robotics and Automation Letters*,

vol. 6, no. 4, pp. 7580-7587, Oct. 2021, doi: 10.1109/LRA.2021.3098811.

[67] H. R. Hassani, A. Mansouri, and A. Ahaitouf, "Design and Application of a Robust Control System of an Autonomous Multi-Rotor Aircraft Using a Perturbation Estimator," *Advances in transdisciplinary engineering*, 2024, doi: 10.3233/atde241234.

[68] H. Zhang, A. Li, and Y. Wang, "Unmanned Autonomous Helicopter Integral Sliding Mode Control and Its Stability Analysis," *Proceedings of the 11th International Conference on Modelling, Identification and Control (ICMIC2019)*, pp. 305-313, 2020, doi: 10.1007/978-981-15-0474-7_29.

[69] Z. M. Manaa, M. R. Elbalshy, and A. M. Abdallah, "Data-driven Discovery of The Quadrotor Equations of Motion Via Sparse Identification of Nonlinear Dynamics," Jan. 2024, doi: 10.2514/6.2024-1308.

[70] R. Tarighi, A. H. Mazinan, and M. H. Kazemi, "Velocity Control of Nonlinear Unmanned Rotorcraft using Polytopic Modelling and State Feedback Control," *International Journal of Advanced Design & Manufacturing Technology*, vol. 13, no. 3, 2020, doi: 10.30495/admt.2020.1881971.1151.

[71] C.-J. Kim, S. H. Lee, and S. W. Hur, "Kinematically Exact Inverse-Simulation Techniques with Applications to Rotorcraft Aggressive-Maneuver Analyses," *International Journal of Aeronautical and Space Sciences*, vol. 21, no. 3, pp. 790–805, Sep. 2020, doi: 10.1007/S42405-020-00249-8.

[72] D. Bicego *et al.*, "Nonlinear Model Predictive Control with Enhanced Actuator Model for Multi-Rotor Aerial Vehicles with Generic Designs," *Journal of Intelligent and Robotic Systems*, vol. 100, no. 3, pp. 1213–1247, 2020, doi: 10.1007/S10846-020-01250-9.

[73] M. Gladfelter, C. He, C. Chang, M. B. Tischler, M. J. Lopez, and O. Juhasz, "Enhancement and Validation of VPM-Derived State-Space Inflow Models for Multi-Rotor Simulation," *VFS 76rd Annual Forum*, 2020, doi: 10.4050/f-0076-2020-16287.

[74] A. Goel and A. K. Manocha, "Balanced Truncation Constrained Order Reduction of Complex Power Systems using Moth Flame Optimization," *2024 15th International Conference on Computing Communication and Networking Technologies (ICCCNT)*, pp. 1-6, 2024, doi: 10.1109/ICCCNT61001.2024.10726177.

[75] O. Axelou, G. Floros, N. Evmorfopoulos, and G. Stamoulis, "Accelerating Electromigration Stress Analysis Using Low-Rank Balanced Truncation," *2022 18th International Conference on Synthesis, Modeling, Analysis and Simulation Methods and Applications to Circuit Design (SMACD)*, pp. 1-4, 2022.

[76] B. B. Duddeti, "Order Reduction of Large-Scale Linear Dynamic Systems Using Balanced Truncation with Modified Cauer Continued Fraction," *IETE Journal of Education*, pp. 1–12, Feb. 2023, doi: 10.1080/09747338.2023.2178530.

[77] M. Rasheduzzaman, P. Fajri and B. Falahati, "Balanced Model Order Reduction Techniques Applied to Grid-tied Inverters In a Microgrid," *2022 IEEE Conference on Technologies for Sustainability (SusTech)*, pp. 195-202, 2022.

[78] U. Zulfiqar, X. Du, Q. Song, and V. Sreeram, "Three Frequency-limited Balanced Truncation Algorithms: A Comparison and Three Families of Extensions," *2022 13th Asian Control Conference (ASCC)*, pp. 1654–1659, May 2022, doi: 10.23919/ascc56756.2022.9828217.

[79] M. S. Hossain and S. Trenn, "Midpoint-Based Balanced Truncation for Switched Linear Systems With Known Switching Signal," in *IEEE Transactions on Automatic Control*, vol. 69, no. 1, pp. 535-542, Jan. 2024.

[80] Y. Yao, Z. Huang, and X. Du, "On the Pole Location of Reduced-order Model in Balanced Truncation Model Order Reduction," *2023 35th Chinese Control and Decision Conference (CCDC)*, pp. 5250-5253, 2023, doi: 10.1109/CCDC58219.2023.10326780.

[81] F. Hilgemann and P. Jax, "Order Reduction of Multi-Channel FIR Filters by Balanced Truncation," *ICASSP 2023 - 2023 IEEE International Conference on Acoustics, Speech and Signal Processing (ICASSP)*, pp. 1-5, 2023.

[82] P. Benner, P. Goyal and I. P. Duff, "Gramians, Energy Functionals, and Balanced Truncation for Linear Dynamical Systems With Quadratic Outputs," in *IEEE Transactions on Automatic Control*, vol. 67, no. 2, pp. 886-893, Feb. 2022, doi: 10.1109/TAC.2021.3086319.

[83] H. Ezoe and K. Sato, "Model Compression Method for S4 With Diagonal State Space Layers Using Balanced Truncation," in *IEEE Access*, vol. 12, pp. 116415-116427, 2024.

[84] S. M. Djouadi, "A Note on the Optimality of Balanced Truncation for a Class of Infinite Dimensional Systems," *2023 American Control Conference (ACC)*, pp. 336-340, 2023.

[85] G. Cai, B. M. Chen, and T. H. Lee, *Flight dynamics modeling*, in *Unmanned Rotorcraft Systems*. Cham: Springer, 2011, pp. 97–135.

[86] Z. Chen, X. Tu, Q. Yang, D. Wang, and J. Fu, "Autonomous trajectory tracking control for a large-scale unmanned helicopter under airflow influence," *Mathematical Problems in Engineering*, vol. 2019, 2019.